Thermodynamic properties of stishovite at mantle conditions determined from pressure variations of vibrational modes

ANNE M. HOFMEISTER

Dept. of Earth and Planetary Sciences, Washington University, St. Louis, MO 63130, U.S.A.

Abstract—Thermodynamic properties were calculated from infrared (IR) spectra of synthetic stishovite that were measured at room temperature and at pressures up to 360 kbar generated by a diamond anvil cell. Two IR modes with 1 atm frequencies ν of 761 and 836 cm^{-1} have nearly constant $d\nu_i/dP$ and initial mode Grüneisen parameters $\gamma_{io} = (K_T/\nu_i)d\nu_i/dP|_o$ near 1, with $d\gamma_i/dP|_o$ less than -0.0005/kbar. Modes initially at 580 and 470 cm^{-1} both show moderate decreases of $d\nu_i/dP$ at high pressures, γ_{io} values near 2, and derivatives $d\gamma_i/dP|_o$ near -0.004/kbar. Averaging all the optic modes gives $\gamma_{ave} = [1.15 \pm 0.04] - [0.0014 \pm 0.0005]*P(kbar)$. The result compares well with the 1 atm high temperature value of $\gamma_{th} = 1.2 \pm 0.1$ and with the initial slope $d\gamma_{Th}dP|_o = -0.002$, which was calculated using the slope dC_V/dP obtained from Kieffer's model, below. The bulk modulus K_T of 3085 ± 25 kbar calculated from only V_o and $\nu_i(P)$ equals the acoustic value within the experimental uncertainties. The calculated dK/dP of 4.1 ± 0.3 is higher than previous determinations but reproduces available V(P) data, suggesting that this new value is correct. The calculated K'' of -0.0009 ± 0.0002/kbar is similar to those previously measured for dense oxides. The above quadratic representation of K(P) can be integrated to predict volumes up to the phase transition at 500 kbar. From previous data on $d\nu_i/dT$, dK/dT is predicted to be -0.185 ± 0.020 kbar/K which is similar to the 1 atm values for many silicates. Heat capacity and entropy calculated from Kieffer's model are in excellent agreement with calorimetric data from 150 to 660 K, suggesting that the calculations can be used to extrapolate C_P and S at temperatures higher than the region of calorimetric measurements. The calculated pressure dependence of C_V is weak at temperatures above 1000 K [e.g., $C_{V,1000K}(J/mol-K) = 73.69 - 0.00097P(kbar)$], whereas the dS/dP is smallest at low temperatures (e.g., $S_{V,298K}$ (J/mol-K) $= 14.51 - 0.0173P + 1.873 \times 10^{-6}$ $P(kbar)^2$). The excellent agreement of calculated macroscopic properties with all available thermodynamic and elastic measurements suggests that the predicted 1 atm quantities (dK/dT, K'', dC_v/dP, dS/dP and $d\gamma_{th}/dP$) are correct and that the above formulations can be extrapolated to mantle conditions with confidence.

INTRODUCTION

ROGER G. BURNS had long-standing interests in mantle minerals and in using spectra to understand the physical properties of materials (see *e.g.,* BURNS' 1970 monograph). He was particularly well-known for his applications of crystal field spectra to problems of chemical composition, phase transitions, and fractionation processes (*e.g.,* BURNS and FYFE, 1967; BURNS, 1985). Vibrational spectra can also be used to constrain thermodynamic properties of solids under conditions that cannot be attained during direct thermochemical measurements. This spectroscopic approach is particularly applicable to mantle petrology because the samples are small and metastable at ambient conditions, and because pressure/temperature conditions appropriate to the mantle are difficult to attain in the laboratory.

At high pressure, SiO_2 adopts the rutile structure (STISHOV and POPOVA, 1961; CHAO *et al.,* 1962). The physical response of stishovite to pressure is of interest because this phase has one of the simplest structures and chemistries of all compounds with Si cations that are octahedrally coordinated by O. Stishovite may be a important constituent of the

Earth's mantle because free SiO_2 in this region could result either from transformation of quartz or disproportionation of a number of common silicate minerals. Therefore, knowledge of the thermodynamic properties of stishovite are needed for geophysical models.

Entropy and heat capacity can be accurately calculated through KIEFFER's (1979; 1980) model if the vibrational data are reasonably complete (*e.g.,* HOFMEISTER and CHOPELAS, 1991). In particular, spectroscopic modeling in conjunction with heat capacities measured over a limited temperature range serve to tightly constrain the entropy. This approach is useful because the volumes of material produced in high pressure syntheses are sufficient for calorimetric measurements at moderate temperatures (300 to 1000 K), whereas cryogenic measurements require dozens of synthesis runs.

Reliable knowledge of bulk moduli and their P and T derivatives for mantle minerals as functions of pressure and temperature are needed to construct a compositional model for the mantle. This may be accomplished through comparing the elasticity measurements to seismological observations. Uncertainties in the pressure derivatives of the bulk
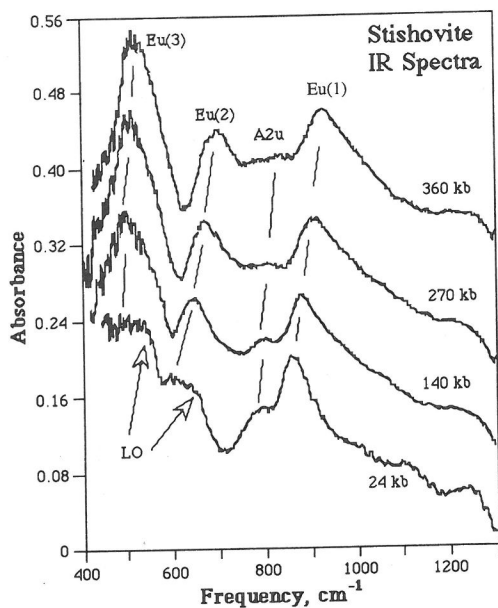
FIG. 1. Infrared spectra of stishovite at pressure. Pressures are labeled in kbar. Peaks are labled by short dashes. The series taken during decompression is shown. The spectra are shifted for clarity. The true absorbances are all nearly the same at 1300 cm⁻¹. Note: these spectra were scanned from hard copies. The resolution of the original spectra was degraded during the process.

modulus arise due to technical difficulties (*e.g.*, limited pressure range) and trade-offs between K and K′ that are made through the equation of state. The latter problems are severe for high-pressure, deep mantle phases with large bulk moduli, such as stishovite. Complementary approaches of deducing derivatives of the elastic moduli are desirable, *e.g.*, through spectroscopy.

This paper presents data on all four IR modes of stishovite from 1 atm to 360 kbar, which is an advance over previous IR data (WILLIAMS *et al.*, 1993) that depicted only two of the modes. The new IR data plus Raman data at pressure of KINGMA *et al.* (1994), and Raman data at temperature of GILLET *et al.* (1990) are used to calculate thermodynamic properties including heat capacity and bulk modulus as functions of temperature and pressure, using the semi-empirical models of KIEFFER (1979; 1980) and HOFMEISTER (1991). Because curvature in $d\nu/dP$ is observed, higher order pressure derivatives, *e.g.* d^2K/dP^2 and $d\gamma/dP$, are also determined.

EXPERIMENTAL

The sample of synthetic stishovite is described by HOFMEISTER *et al.* (1990a). Pressure was generated by a Mao-

Bell diamond anvil cell (DAC) with type II stones. A thin film of stishovite was prepared by compressing powder with an ungasketed DAC. A preindented stainless steel gasket with a 200 μm aperture was mounted on the diamond with the sample. The aperture was filled with CsI for a pressure transmitting medium, and a dozen small (ca. 5 μm) ruby grains were sprinkled on top of the CsI. Pressure was determined by using the ruby fluorescence technique (*e.g.*, MAO *et al.*, 1986) and by averaging the pressure values for eight grains which were evenly scattered across the surface of the CsI. Mid-IR spectra were collected at a resolution of 1 cm⁻¹ using a Nicolet 7199 optical bench, a Nicolet 1280 data processor, a KBr beamsplitter, and a HgCdTe detector. The number of scans varied from 5,000 to 44,000, such that longer collection times were used for the higher pressure runs in order to improve the signal-to-noise ratio. A detailed description of the procedures is given by HOFMEISTER *et al.* (1989).

RESULTS

Mid-infrared spectra of synthetic stishovite taken at quasi-hydrostatic pressures from 1 atm to 360 kbar posses three strong bands, one weak band, and a few shoulders whose frequencies ν all gradually increase with pressure (Fig. 1; Table 1). This intensity pattern (Fig. 1) is consistent with symmetry analysis (TRAYLOR *et al.*, 1971) and reflectivity measurements of various compounds with the rutile structure (HOFMEISTER *et al.*, 1990a,b). The three strong peaks represent the three modes with E_u symmetry and the weak band is associated with the single A_{2u} mode. The shoulders are the longitu-

Table 1. IR frequencies of stishovite vs. pressure

Pressure Kbar	Volume cm³/mole	$E_u(1)$ cm⁻¹	A_{2u} cm⁻¹	$E_u(2)$ cm⁻¹	$E_u(3)$ cm⁻¹
0.001[1]	14.016	836		580	470
15±1	13.948	841.7	760	593	470
45±4	13.817	850.0	758	599	489
30±2	13.881	850.0	766	596	489
56±3	13.770	854	772	609	482±4
70±3	13.709	856	775	615	479±2
97±3	13.590	864±2	781	619	497
117±3	13.518	865±2	784	634±2	498
127±4	13.480	873	785	635±5	492±4
144±5	13.414	875	788	642	496
160±8	13.353	880	792±2	636±3	505±2
175±10	13.298	881	795	642±2	498±4
200±10	13.207	885	797	646	505±5
212±10	13.162	882	800	649	?
235±10	13.085	889	800	654±3	510±5
269±15	12.968	903	805	671±2	507±5
300±15	12.867	910	816±5	680±2	513±5
335±15	12.755	915	818±5	685±3	512±5
360±15	12.677	920	830±3	695±2	515±2
270±15	12.965	901±2	802	665±4	506±4
140±10	13.429	871	790±2	637±3	494±3
8±1	13.980	840±5	767	579±2	?
24±1	13.907	848	768±3	590	?

[1] Thin film frequencies from HOFMEISTER *et al.* (1990)

dinal optic (LO) components. These shoulders appear to follow the same trends as the strong peaks. However, the data are not presented here because the shoulders could not be traced over a pressure range that was sufficiently wide to accurately establish the slope $d\nu/dP$. The position of the lowest frequency E_u peak could not be determined from some of the low pressure runs (Table 1) due to a combination of two effects: interference fringes were present in a few runs, and this peak is located near the cut-off of the detector and beamsplitter.

The peaks broaden and decrease slightly in intensity such that the area is roughly constant during the decompression runs. Because only three spectra were acquired during decompression and because samples thin during compression, quantitative analyses of the pressure dependence of peak width, intensity, or area are not presented.

The pressure dependence of the two low frequency IR modes is clearly non-linear (Fig. 2), such that the slope $d\nu/dP$ decreases as pressure increases. This behavior has been previously observed (*e.g.*, HOFMEISTER *et al.*, 1989) and represents the increasing resistance of the structure to compression. Least squares analysis shows that the data are well described by a quadratic fit (Table 2). The initial frequencies were constrained from the previous thin film and reflectivity measurements (HOFMEISTER *et al.*, 1990a) in order to obtain the most accurate value for the initial slope. Similar fits were obtained by allowing ν_o to vary and the resultant parameters lie within the uncertainty of those reported in Table 2.

Peak positions of the two high frequency peaks depend nearly linearly on pressure (Fig. 2). The $E_u(1)$ peak shows a slight, but measurable, curvature near 1 atm. Because the data at low pressures have the least experimental uncertainties, a quadratic fit and a fixed initial frequency (Table 2) are reported for the least squares analysis. The initial slope of 0.28 cm^{-1}/Kbar for the quadratic fit is slightly higher than the slope of 0.22 cm^{-1}/Kbar derived from the linear fit, which is consistent with negative curvature.

For the weak A_{2u} peak, the 1 atm position was not clearly discerned in the thin film experiment. Therefore, least squares analysis and a linear fit were used to constrain its 1 atm position. The resulting value of 761 cm^{-1} (Table 2) is higher that the TO position of roughly 670 cm^{-1} derived from reflectivity data (HOFMEISTER *et al.*, 1990a). Because the A_{2u} peak is very broad in rutile compounds (*e.g.* GeO$_2$: KAHAN *et al.*, 1971; ROESSLER and ALBERS, 1972), the absorption peak should occur at a considerably higher frequency than the TO position (WOOTEN, 1972). The slope derived from the linear fit represents a lower limit because this mode probably depends quadratically on pressure as did the three E_u modes.

COMPARISON WITH PREVIOUS SPECTROSCOPIC MEASUREMENTS

IR spectra of stishovite were previously collected from 0.5 to 2 μm size grains dispersed in CsI to pressures of 360 kbar with pressures determined from three to six grains of ruby (WILLIAMS *et al.*, 1993). The spectra presented of stishovite have the three E_u peaks and several shoulders (see Fig. 6 in WILLIAMS *et al.*, 1993). However, the intensity of $E_u(2)$ is high relative to the other peaks, the peaks are asymmetrically shaped, and the positions are about 30 cm^{-1} higher than ours at the same pressure. The differences are clearly due to sampling from a dispersion: (1) scattering contributes an LO component, causing the asymmetric profile and the shift of the maximum to higher wavenumbers than
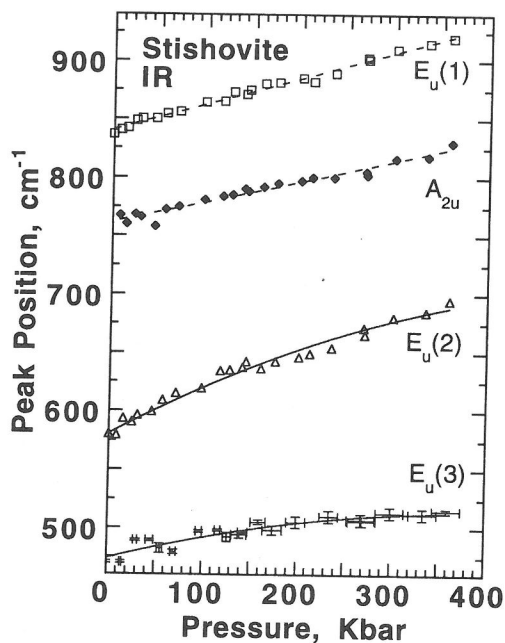

FIG. 2. IR peak positions of stishovite as a function of pressure. Dashed lines, linear fits to the data. Solid lines, quadratic fits to the data. Open square, $E_u(1)$. Filled diamond, A_{2u}. Open triangle, $E_u(2)$. Plus sign, $E_u(3)$. Error bars are shown for the lowest frequency peak. For the other modes, the uncertainty in frequency is generally less than or equal to the size of the symbol. The errors in pressure are less than the size of the symbol for P below 100 kbar, and as indicated for $E_u(3)$ at higher pressures.

Table 2. Pressure dependencies of vibrational modes in stishovite.

Mode	ν_0 cm^{-1}	$d\nu/dP$ cm^{-1}/kbar	$d^2\nu/dP^2$ cm^{-1}/kbar^2	R	χ^2
IR					
$E_u(1)$ [1]	836.0[2]	0.28 ±0.01	-0.00015±0.00005	0.99	200
A_{2u}	761.4±1.5	0.176±0.008		0.98	318
$E_u(2)$	580.0[2]	0.44 ±0.02	-0.00038±0.00007	0.99	588
$E_u(3)$	470.0[2]	0.25 ±0.02	-0.00036±0.00007	0.93	443
Raman [3]					
B_{2g}	966.2[4]	0.383±0.006	-0.00009±0.00001	0.99	27
A_{1g}	754.1[4]	0.311±0.008	-0.000025±0.00002	0.99	75
E_g	589.0[4]	0.217±0.003	-0.000067±0.00006	0.99	11
B_{1g}	231.6[4]	-0.102±0.002	-0.000068±0.00005	0.99	5

[1] The linear fit (840.4±0.9)+(0.225±0.005)*P has R=0.99 and χ^2=148. [2] The initial frequencies were constrained from reflectance and thin film data of HOFMEISTER et al. (1990a). [3] Least squares analysis of data from KINGMA et al. (1994). [4] The initial frequencies were set to the 1 atm values of HEMLEY (1987) and KINGMA et al. (1994).

the TO position, (2) variations in crystal size cause weaker peaks to appear more intense than they should be, and (3) the grain sizes are larger than the sub-micron thickness needed to transmit light through a silicate mineral (for a detailed comparison of spectra produced from dispersions and thin films see HOFMEISTER, 1995). Furthermore, as the pressure changes, the change in intensity observed from the present study of thin films (Fig.1) means that a different proportion of LO and TO components are sampled as pressure increases. The degree to which this occurs depends on distribution of particulate sizes and the rate of change of intensity with pressure. There appears to be increased sampling of the LO component over the TO with pressure in the data of WILLIAMS et al. (1993) because their reported trends for E_u(1) and E_u(2) are linear (trends for the other two peaks are not presented). Other reasons for curvature not being observed in the previous data set are (1) the curvature is most apparent at low pressure (Fig. 2) but WILLIAMS et al. data are sparse in that pressure region; and (2) determination of slight amounts of curvature requires accurate 1 atm values, whereas WILLIAMS et al. data is not as well constrained at 1 atm. Moreover, the pressures of WILLIAMS et al. study may not be as accurate as those reported here, because fewer ruby grains were used in computing the average pressure.

Raman modes of stishovite were acquired at pressures of up to 328 kbar (HEMLEY, 1987) and up to 500 kbar by KINGMA et al. (1994). The frequencies of the lower pressure data set appear to linearly depend on pressure, but the data set acquired over a larger pressure range shows curvature for all four modes, such that the lower frequency modes have more curvature (see Fig. 2 in KINGMA et al., 1994). The values for $d^2\nu/dP^2$ in Table 2 were calculated from quadratic fits for pressures from 1 atm to 410 kbar to KINGMA et al's. data (K. KINGMA, pers. commun. 1995). The data set was truncated because a phase transition occurs near 500 kbar. The frequency of the B_{1g} mode has a negative pressure shift (HEMLEY, 1987). This soft mode behavior is particular to the B_{1g} mode as its atomic motions (see TRAYLOR et al., 1971) lead to a shear-type distortion of rutile to the CaCl$_2$ structure (NAGEL and O'KEEFE, 1971). Thus, the behavior of the Raman bands is entirely consistent with the response of the IR bands to pressure reported here.

MODE GRÜNEISEN PARAMETERS AND THEIR PRESSURE DERIVATIVES

Mode Grüneisen parameters were calculated from

$$\gamma_i = \frac{K_T}{\nu_i} \frac{\partial \nu_i}{\partial P} \qquad (1)$$

where K_T is the bulk modulus. We first discuss the initial values of γ_i, and then their pressure derivatives. An initial value K_{T_0} of 3060 Kbar established by Brillouin scattering techniques (WEIDNER et al., 1982) was applied both to the IR data from this work and to previous measurements of the Raman modes (HEMLEY, 1987; KINGMA et al., 1994). The

initial mode gammas are calculated from eqn. (1), rather than from the volume dependence, because this approach gives an accurate initial value, minimizes manipulation of the spectroscopic data, and relies the least upon the equation of state.

The high frequency IR modes have low initial values ($\gamma_{io} \sim 1$, Table 3), which are similar to the behavior of the E_g bending mode that is active in the Raman (HEMLEY et al., 1986; KINGMA et al., 1994). Low values of γ_{io} for A_{2u} and E_g are consistent with their atomic motions lying along the c axis (TRAYLOR et al., 1971) which is less compressible than the a axis (WEIDNER et al., 1982). The A_{1g} and B_{2g} modes active in the Raman have similar stretching motions involving Si cations moving against a stationary O sublattice (TRAYLOR et al., 1971) and similar intermediate values (HEMLEY et al., 1986; KINGMA et al., 1994). The $E_u(1)$ motions are closely related to those of the A_{1g} and B_{1g} Raman modes in that the Si and O sublattices move in opposite directions in $E_u(1)$. A value of 1 for γ_{io} is thus reasonable for $E_u(1)$. In contrast, the low frequency IR modes have high initial values ($\gamma_{io} \sim 2$, Table 2). High values of γ_{io} for $E_u(2)$ and $E_u(3)$ are consistent with their atomic motions involving stretching along the a axis (TRAYLOR et al., 1971). These motions differ significantly from that of $E_u(1)$, B_{2g} and A_{1g} in that pairs of O and Si move together in the former, whereas in the latter O and Si move in opposite directions. The B_{1g} mode in the Raman has a very different negative γ_{io} (see summary in Table 3), as expected for this soft mode.

That similar values of γ_{io} are found for modes with similar atomic motions suggests that mode Grüneisen parameters can be predicted for the inactive modes. By comparing the atomic motions of the modes as derived by TRAYLOR et al. (1971), we predict that the inactive $B_{1u}(1)$ and (2) modes which are derived from atomic motions along the c axis will have γ_{io} values like those of A_{2u} and E_g; respectively. A_{2g} could either have a have a γ_{io} about 0.4 larger than those of B_{2g} and A_{1g} (because γ_{io} of E_g is 0.4 larger than that of A_{2u}) or a γ_{io} that is 0.4 higher than that of E_g (because γ_{io} of $E_u(1)$ is 0.4 larger than that of A_{2u}). The value given is Table 3 is the average of these possibilities.

The pressure dependence of γ_i for each of the IR and Raman modes was calculated from the quadratic fits of Table 2 and by approximating the bulk modulus as:

$$K_T = K_{To} + K' P \qquad (2)$$

where the pressure derivative K' of 2.8 ± 0.2 determined by ROSS et al. (1990) was used. ROSS et al. (1990) derived this value for K' by combining their V(P) data with the ultrasonic measurement of K_{To} by WEIDNER et al. (1982). This combination of data sets constrains K' value better than V(P) data alone (BASS et al., 1981). The polynomial approach is used to calculate γ_i because it results in the best constraint of the initial value for $d\gamma/dP|_o$

Table 3. Mode Grüneisen parameters for stishovite

Mode	Description	v_o cm^{-1}	γ_{io}[1]	$d\gamma_i/dP\,\vert_o$[2] kbar^{-1}
IR				
$E_u(1)$	Stretch(Si vs. O) ∥a	836.0[3]	1.03±0.04	-0.0005±0.0001
A_{2u}	Stretch(Si vs. O) ∥c	761.4±1.5	0.71±0.03	~0
$E_u(2)$	Stretch ∥a	580.0[3]	2.3 ±0.1	-0.0036±0.0006
$E_u(3)$	Stretch ∥a	470.0[3]	1.6 ±0.1	-0.0040±0.0008
Raman				
B_{2g}	Stretch(Si vs. O) ∥a	966.2[4]	1.21±0.02[5]	~0
A_{1g}	Stretch(Si vs. O) ∥a	754.1[4]	1.26±0.03[5]	~0
E_g	Bend ∥c	589.0[4]	1.12±0.01[5]	-0.0001±0.0001
B_{1g}	Shear ∥a	231.6[4]	-1.34±0.03[5]	-0.0040±0.0008
Inactive				
A_{2g}	Bend ∥a	671[6]	1.6[7]	~0[7]
$B_{1u}(1)$	Bend ∥c	515[6]	1.1[7]	~0[7]
$B_{1u}(2)$	Stretch ∥c	143[6]	0.7[7]	~0[7]

[1] K_{To} of 3060 kbar was used (WEIDNER et al., 1982). [2] K' of 2.8 was used (ROSS et al., 1990). [3] The initial frequency is from HOFMEISTER et al. (1990a). [4] The initial frequency was constrained by data from KINGMA et al. (1994). [5] From a quadratic fit to the data of KINGMA et al. (1994). [6] Predicted from systematics (HOFMEISTER et al., 1990b). [7] Predicted from modes with similar atomic motions: see text.

The calculated γ_i (Fig. 3) values for the IR modes clearly exhibiting curvature in $d\nu/dP$ decrease as pressure increases, as expected from the definition (eqn. 1). The decrease in $E_u(1)$ is an order of magnitude less than those for $E_u(2)$ and (3), consistent with the relative degrees of curvature. The calculation indicates that γ_i may not linearly depend on pressure; however, because the curvature in γ_i with P is slight (Fig. 3) and because eqn. (2) is a first order approximation in pressure, it is appropriate to model the slope $d\gamma_i/dP$ as a constant (Table 3). For A_{2u}, the increase in γ_i with pressure is an artifact of the linear dependence of frequency with pressure. The derivative $d\gamma_i/dP$ is therefore close to zero (Table 3): it can be no larger than that of $E_u(1)$.

The Raman modes behave similarly (Fig. 3, Table 3). The slope $d\gamma_i/dP$ is less and approaches zero for several of the modes, resulting in nearly constant mode gammas. The increase in γ_{io} for A_{1g} results because curvature of $\nu(P)$ equals 0 within experimental uncertainty. The soft mode B_{1g} has a large slope similar to those of $E_u(2)$ and $E_u(3)$.

The mode gammas of the inactive modes were assumed to be independent of pressure. This approximation is reasonable in that $d\gamma_i/dP$ is near 0 for most of the Raman and IR modes (Table 3).

CALCULATION OF THERMODYNAMIC AND ELASTIC PROPERTIES

Bulk modulus and its pressure derivatives

Elastic properties can be calculated from vibrational frequencies (BROUT, 1959). The assumptions are electrostatic attractive forces, pair-wise central repulsive forces, rigid ions, and a structure which scales upon compression. The relation for compounds with the rutile structure is (HOFMEISTER, 1991):

$$K_T(P) = \frac{4P}{3} + \frac{0.0006554}{V} r_o^2 \sum_{i=1}^{18} \nu_i^2(\bar{k}) \quad (3)$$

where the numerical constant incorporates the reduced mass, coordination numbers, and physical constants and give K_T in kbar; P is pressure in kbar, V is the unit cell volume in $\mathring{A}^3$; and r_o is the average Si-O distance in $\mathring{A}$ The sum can be taken at any point in the Brillouin zone: zone center is most convenient and thus the sum involves only the 15 optic modes. The LO and TO components of A_{2u} count as $\frac{1}{2}$ mode each, whereas those of the E_u modes count as 1 mode each in order to properly account for degeneracy. In the calculation, we take advantage of the fact that r_o^3 maintains its 1 atm proportionality with V, that is the shape of the Si octahedron was not found to change with pressure (ROSS et al., 1990). This observation allow elimination of r_o from eqn. (3).

The strong dependence of bulk modulus on frequency but weak dependence on volume (as $V^{1/3}$) or bond length, also allows $K_T(P)$ to be calculated independently of the equation of state through iteration. A trial function for $K_T(P)$ is obtained by substituting only $\nu_i(P)$ and one volume at one specific pressure (1 atm in this case) into eqn. (3); this result is integrated using:

$$V(P) = V_o \exp\left\{-\int_0^P \frac{dp}{K_T(p)}\right\} \quad (4)$$

to give V(P), which is then substituted into eqn. (3) with $\nu_i(P)$ to redetermine $K_T(P)$; these steps are repeated until iteration no longer changes V(P) or $K_T(P)$.

Implicit in equations (3) and (4) are that all quantities are measured at the same temperature. For determinations of dK/dP and d^2K/dP^2, room temperature is used. The spectroscopic data and esti-
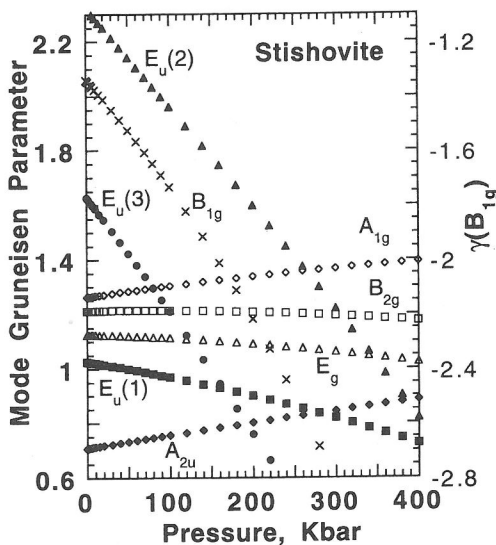

FIG. 3. Mode Grüneisen parameters of stishovite as a function of pressure. Filled triangle, $E_u(1)$. Filled square, $E_u(2)$. Filled circle, $E_u(3)$. Filled diamond, A_{2u}. Open diamond, A_{1g}. Open square, B_{2g}. Open triangle, E_g. X, the soft mode B_{1g}. The scale on the right side pertains only to B_{1g}. The increase in γ_{io} for A_{2u} is an artifact of using a linear fit for $\nu(P)$. The increase in γ_{io} for A_{1g} results because curvature of $\nu(P)$ equals 0 withing experimental uncertainty.

mates are given in Tables 2 and 3. The initial volume of 46.61 Å^3 of HILL et al. (1983) was used.

The calculated initial value K_{To} equals 3085 ± 25 Kbar, which lies midway between and within the experimental uncertainty of the acoustic determination of WIEDNER et al. (1982) and of the volumetric determination of ROSS et al.'s (1990). The present value is slightly lower than that of HOFMEISTER (1991) because the inactive modes in this work were derived from trends of all known rutile-type compounds (HOFMEISTER et al., 1990b), whereas the previous estimates were made based on data for TiO_2 only. The agreement for compounds with the rutile structure is generally good (HOFMEISTER, 1991) because (1) the vibrational sums are well-constrained, and (2) the like atoms are further than second-nearest neighbors, suggesting that the assumed forms of the potentials are reasonable.

The accuracy of the pressure determination is clearly shown in the volume determination. Volume derived solely from V_o and $\nu_i(P)$ is in superb agreement with experiment at pressures below 130 kbar (Fig. 4). Above 130 kbar, the data points fall below the calculated V(P) curve, deviating 0.2% at 150 kbar. However, the calculation lies within the experimental uncertainty of all data points except the one at 150 Kbar. The small discrepancy for that data point could result if the uncertainty in the pressure determination were larger than ±1 kbar. A small systematic error could be present for this datum as it was the last measurement in one of the runs. In particular, a slight reduction in hydrostaticity is likely present as the methanol-ethanol mixture is known to become increasingly stiff above 100 kbar. The comparison suggests that the volume obtained by integrating the vibrational frequencies (eqns. 3 and 4) lies within 0.1% of the actual value. An equation for V(P) can be obtained by interating eqn. (5), below.

The pressure dependence of K_T which was derived solely from $\nu_i(P)$ and V_o (Fig. 4) is closely described by the quadratic equation:

$$K_T(P) = 3084.5 + (4.103 \pm 0.003)\,P$$
$$- (0.000866 \pm 0.000008)\,P^2. \quad (5)$$

The low uncertainties in eqn. (5) reflect the goodness of the fit. The value of K' calculated from spectroscopic measurements is 4.1 ± 0.3, considering the uncertainties in $d\nu_i/dP$. The spectroscopic determination for K' is larger than the value of 2.8 that Ross et al. (1990) derived from V(P) data assuming the acoustic value for K_{To}. However, V(P) data do not constrain both K and K' (the quantities are interrelated through the chosen equation of state). As shown in Fig. 4, the V(P) data of ROSS et al. (1990) can be described by $K' = 4$ in a Birch-Murnaghan equation if $K_{To} = 3006 \pm 18$ kbar, which is within the uncertainty of the acoustic value. In contrast, the values of K, K' and K" derived from spectroscopic data are independent. It thus appears that stishovite has a K' value similar to that observed for the majority of silicate phases. A more precise determination of K' could be made by combining the spectroscopic calculation with one accurate determination of volume at high pressure (ca. 300 kbar) under hydrostatic conditions.

The calculated value for K" of −0.0009 ± 0.0002/kbar is similar those measured for Mg_2AlO_4 with K" of −0.065/kbar (CHANG and BARSCH, 1973; YONEDA, 1990); and for MgO with K" of −0.006 ± 0.003/kbar (JACKSON and NIESLER, 1982) or −0.003 to +0.001 (YONEDA, 1990). To my knowledge, no other data on K" exists for materials chemically or structurally similar to stishovite. Because K" correlates roughly inversely with the bulk modulus (see discussion of alkali halides in HOFMEISTER, 1991) and because K_{To}'s are 3060 kbar for SiO_2, 1964 kbar for $MgAl_2O_4$, and 1603 kbar for MgO, the calculated K_o'' of stishovite appears to be reasonable.
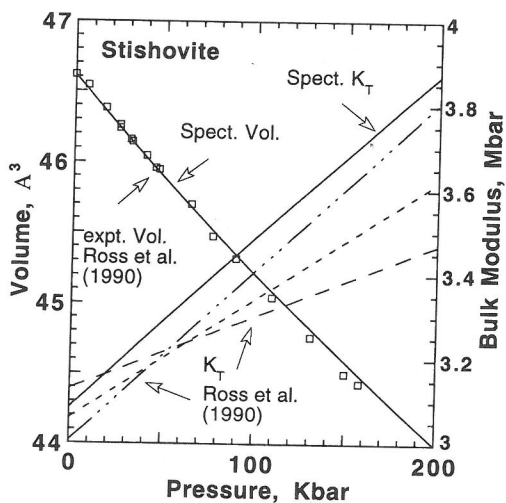

FIG. 4. Volume and bulk modulus of stishovite as a function of pressure. Solid lines, spectroscopic calculation based on V_o and $\nu_i(P)$. Open squares, data from ROSS et al. (1990). Short dashed line, K(P) from Birch-Murnaghan fit to the V(P) data with K_{To} set to the acoustic value. Dot-dashed line, K(P) from Birch-Murnaghan fit to the V(P) data with K' set to 4. Long dashed line, K(P) from Birch-Murnaghan fit to the V(P) data allowing both parameters to float.

Temperature derivative of the bulk modulus and the Anderson-Grüneisen parameter

For determination of dK/dT, ambient pressure and the temperature variations of the volume measured by ENDO *et al.* (1986) were used in eqn. (3). Temperature variations of the Raman modes have been measured by GILLET *et al.* (1990). The peak positions depend linearly on temperature with slopes of -0.022 ± 0.002 cm^{-1}/K for A_{1g}, -0.014 ± 0.002 cm^{-1}/K for E_g, and 0 for B_{1g}. These slopes are roughly -0.068 times the numerical value of $d\nu_i/P$ (KINGMA *et al.*, 1994: see Table 3), allowing estimation of the temperature variations for the other modes from the data in Table 2.

The calculated $K_T(T)$ depends linearly on temperature (Fig. 5) with a slope of -0.185 ± 0.020 Kbar/K. The reported error stems from the uncertainty in the measured variations of the vibrational frequencies with temperature, but does not account for systematic differences between the measured Raman modes and estimated IR modes. The linear trend is due to the linear behavior of frequency with temperature, low slopes for $d\nu_i/T$, and the dominant contribution of ν_i in eqn. (3). No data on dK/dT for stishovite exist to my knowledge for comparison. Rutile has a considerably larger magnitude, -0.41 kbar/K (MANGHNANI, 1969) which is not common for solids. Our determination is similar to measured values commonly observed for dK/dT, *e.g.*, -0.27 kbar/K for MgO (ISAAK *et al.*, 1989) and -0.16 kbar/K α-Mg$_2$SiO$_4$ (SUMINO *et al.*, 1977).
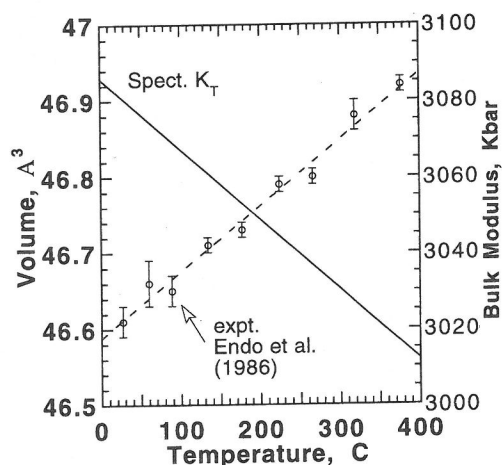

FIG. 5. Volume and bulk modulus of stishovite as a function of temperature. Open circles, volume data of ENDO *et al.* (1986). Dotted line, least squares fit to V(T). Solid line, $K_T(T)$ calculated from V_o and $\nu_i(T)$.

The Anderson-Grüneisen parameter is

$$\delta_T = \frac{-1}{\alpha K_T} \frac{\partial K_T}{\partial T}\bigg|_P \qquad (6)$$

where α is thermal expansivity. The above result and V(T) data of ENDO *et al.* (1986) give δ_T equal to 3.3 ± 0.3 from 300 to 700 K. The predicted value for stishovite is significantly lower than the high temperature values near 5 for a variety of materials (ANDERSON *et al.*, 1990). One possibility is that dK/dT is low because $d\nu_i/dP$ of the IR modes are larger than that predicted from the Raman dependencies. Alternatively, stishovite may have a different value for δ_T because this material has ^{VIII}Si rather than ^{IV}Si and a bulk modulus that is 50% higher than those of the compounds previously investigated.

Construction of density of states for Kieffer's model

KIEFFER (1979; 1980) developed a model based on lattice dynamics that allows calculation of the lattice contribution to C_V and S from vibrational frequencies and acoustic velocities. A model for density of states $g(\nu)$ is constructed as follows. The primitive cell has 3N total degrees of freedom, where N is the number of atoms in a primitive cell. Three of the 3N vibrational modes are acoustic: their frequency values are constrained by the acoustic velocities of the one longitudinal and the two shear waves measured by WEIDNER *et al.* (1982). KIEFFER's (1979) model assumes that frequency ν of the acoustic modes varies sinusoidally with wavevector **k,** a phenomena termed dispersion). The contribution of the acoustic modes occurs at low temperature because the acoustic frequencies are low.

The remaining modes are optic. The density of states in KIEFFER's (1979) model is constructed by distributing the zone center vibrational modes into several continua and Einstein oscillators. The three inactive modes were estimated (Table 3) from systematics of rutile-type structures (HOFMEISTER *et al.*, 1990b). Dispersion is ignored for the optic modes because it is unknown. For solids with a large number of optic modes this assumption contributes a minor error to the calculation because some modes disperse to higher frequencies, and others to lower. Twenty different models for $g(\nu)$ were investigated. Figure 6 shows the preferred model which separately enumerates most of the modes. Two of the inactive modes were estimated to fall within the TO and LO components of the
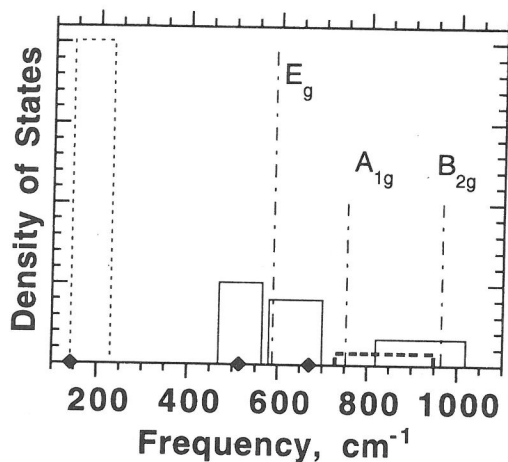
FIG. 6 Model density of states in arbitrary units. Dot-dashed lines with lables, Einstein oscillators representing three of the Raman modes. Solid lines, continuua representing the E_u modes. Thick dashed line, the continuum representing A_{2u}. Dotted lines, the continuum representing $B_{1u}(2)$ and B_{1g}. Solid triangles, positions of the three inactive modes. Relative heights of the three Einstein oscillators are correct, and relative heights of the continuua are correct, but the vertical scales differ for these two representations.

lower frequency E_u modes and thus their estimated frequencies will not affect the calculation. However, the lowest frequency inactive mode is estimated to lie below the lowest frequency Raman or IR modes, and thus its position influences the calculation, especially at low temperature.

If powder data are used, the model usually reproduces heat capacities C_P to within 5% at 298 K and 1% at 700 K. However, the accuracy considerably improves if single-crystal data and band assignments are used to construct the density of states. For example, the existence of a large number of modes over a small interval for olivines or garnets together with well-established band assignments, results in very low uncertainties (0.5%, *e.g.,* HOF-MEISTER and CHOPELAS 1991). Considering (1) that number of modes (15 optical) is moderate, (2) that all but the $B_{1u}(2)$ mode are well constrained, and (3) that dispersion measured for rutile is low to moderate (TRAYLOR *et al.,* 1971), the uncertainty of the calculated values is estimated as <2% from 200 to 800 K.

Calculations can be compared to calorimetric measurements of heat capacity via the anharmonic correction:

$$C_P = C_V + TV\alpha^2 K_T \qquad (7)$$

where V is volume, and α is the thermal expansivity. Single crystal volume is from SINCLAIR and

RINGWOOD (1978) and HILL *et al.* (1983). K_T is from WEIDNER *et al.* (1982). Thermal expansivity of $1.863 \times 10^{-5}/K + (T-273)* 0.344 \times 10^{-10}/K^2$ was determined from a least squares fit to the data of ENDO *et al.* (1986). ENDO *et al.*'s (1986) result lies within the experimental uncertainty of the previous α by ITO *et al.* (1974ab). The temperature dependence of K_T calculated above was used. Given the uncertainties in the temperature derivatives, the entropy is also approximated from

$$S = S_V + TV\alpha^2 K_T \qquad (8)$$

where S_V is the harmonic entropy calculated by the model. Because the anharmonic correction is about 3% of C_P or S, uncertainties in the parameters used contribute little (ca 0.3%). The cumulative uncertainties for the calculated S and C_P should be ~2% from 200 to 800 K.

Heat capacity, entropy, and Debye temperature

The calculated heat capacity (Fig. 7; Table 4) lies within the experimental uncertainty of the scanning calorimetric data of WATANABE (1982). Calculated C_P is equal to the cryogenic data of HOLM *et al.* (1967) within experimental uncertainties at temperatures greater than 150 K (Fig. 7). At low temperatures below 100 K, the discrepancies are greatest, which is typical of KIEFFER's model (*e.g.,* HOFMEISTER and CHOPELAS, 1991). For the case of stishovite, this discrepancy is partially due to estimation of the lowest frequency mode (Fig. 6). The
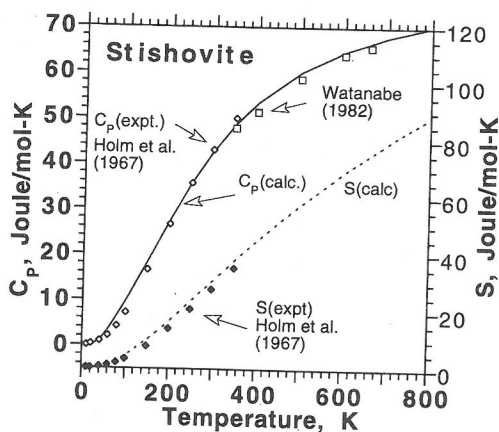

FIG. 7. Heat capacity and entropy of stishovite at 1 atm. Open diamonds, calorimetric data on C_P from HOLM *et al.* (1967). Open squares, calorimetric data on C_P from WATANABE (1982). Solid line, C_P calculated from spectroscopy. Dotted line, S calculated from spectroscopy. The axis on the right hand side refers to the entropy.

Table 4. Thermodynamic properties of stishovite at 1 atm

Temp.	Anharmonic correction	C_P Calculated	Expt.[1]	Expt.[2]	Del[3]	S Calculated	Expt.[2]	Del[3]	γ_{Th}	Debye Temp. Calculated
K	J/mol-K	J/mol-K	J/mol-K	J/mol-K	%	J/mol-K	J/mol-K	%		K
10	0.00126	0.0050		0.0511	90	0.0025	0.0163	85		1182
20	0.00352	0.0387		0.266	85	0.0136	0.112	88		1093
40	0.0766	0.945		0.928	-1.8	0.273	0.476	43		754
60	0.115	3.434		2.175	-58	1.086	1.065	-2		723
80	0.153	6.541		4.265	-53	2.495	1.954	-28		766
100	0.191	9.741		7.173	-36	4.295	3.206	-34		825
150	0.304	18.34		16.55	-11	9.849	7.814	-26		943
200	0.417	27.41		26.59	-3.1	16.38	13.96	-17		1014
250	0.542	35.74		35.66	-0.2	23.43	20.90	-12		1055
298	0.679	42.68		43.03	0.8	30.36	27.82	-9	1.89	1079
350	0.827	48.73	47.77	49.90	2.3[4]	37.72	35.28	-7	1.66	1099
400	0.974	53.4	51.33		-4.0	44.57			1.51	1108
500	1.30	60.18	58.66		-2.6	57.33			1.34	1125
600	1.68	64.72	63.90		-1.3	68.83			1.24	1134
660			65.62							1134
700	2.08	67.92				79.17			1.18	1134
800	2.55	70.32				88.55			1.14	1144
1000	3.59	73.78				111.7			1.09	1140
1500	7.08	79.82				137.5			1.02	1140
2000	12.0	85.67				163.5			0.97	1140

[1] WATANABE (1982).   [2] HOLM et al. (1967).   [3] Del. = (expt.-calc.)/expt.   [4] The % difference for WATANABE'S (1982) data are +2.0.

match with experiment could be improved by using this lower cutoff as a fitting parameter.

The calculated entropy (Fig. 7) is slightly and uniformly higher than HOLM et al.'s (1967) data from temperatures of 100 K to their upper limit of measurement. This behavior is due to the slight mismatch of C_P near 100 K. As errors in S are additive due to the form of the integral defining S, the calculated values above 200 K in Table 4 should be reduced by 2.3 Joule/mol-K, representing the difference between experiment and calculation at 200 K.

The Debye temperature (Table 4; Fig. 8) varies slightly at temperatures above 150 K, increasing gradually form 1000 to 1140 K. Below 150 K, the calculation is not accurate because the cryogenic temperature dependences of the bulk modulus or sound velocities are not known.

Pressure dependence of heat capacity and entropy

Heat capacity and entropy were calculated as functions of pressure by utilizing the measured dependence of the optical frequencies on pressure and by applying the pressure dependence for bulk modulus to the sound velocities of WEIDNER et al. (1982). The latter approximation affects the low temperature values of S and C_V and becomes unimportant above 200 K. The calculated C_V values depend weakly on pressure (Fig. 9). The slope and the curvature in dC_V/dP decrease as temperature increases. Near 2000 K, heat capacity is essentially independent of pressure. Least squares fits are given in Table 5.
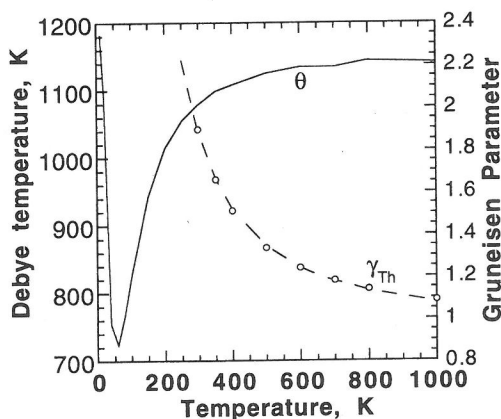

FIG. 8. Thermal Grüneisen parameter (dots) and Debye temperature (solid line) as a function of temperature. The dashed line is the least squares fit to γ_{Th}. The axis on the right hand side refers to γ only.
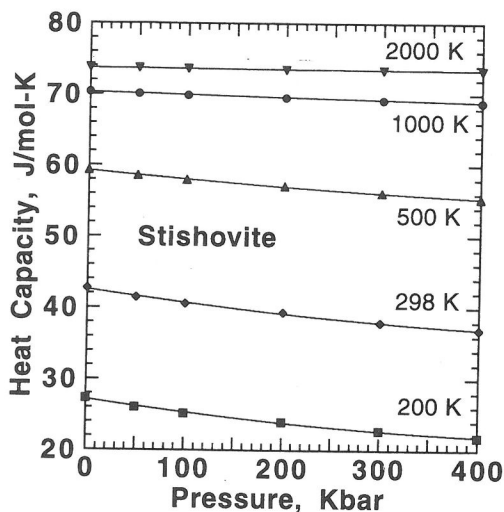
FIG. 9. C_v as a function of pressure. Solid lines are least squares fits to the calculation. Symbols are the calculated values at selected temperatures and pressures. The slope and the curvature decrease as temperature increases. By 2000 K, heat capacity is essentially independent of pressure.

Entropy (Fig. 10) behaves in the opposite manner due to its definition. Curvature is apparent at all temperatures except the lowest (Table 5).

The data in Table 3 and the equations in Table 5 allow extrapolation of S_V and C_V to mantle conditions. S and C_P can be obtained by adding the 1 atm anharmonic correction. The effect of pressure on $TV\alpha^2K_T$ is not significant and lies within the uncertainty of the calculated pressure dependence of C_V and S_V.

Grüneisen parameters and their pressure dependence

The thermal Grüneisen parameter is defined as

$$\gamma_{th} = \alpha K_T V/C_v. \quad (9)$$

Use of $\alpha = 18.5 \times 10^{-6}$/K from ENDO *et al.* (1986), V = 14.02 cm^3/mole from HILL *et al.* (1981), K_T

= 3060 kbar from WEIDNER *et al.* (1982) and C_V =42.4 J/mol-K from HOLM *et al.* (1967) gives γ_{th} equal to 1.89 $\pm$ 0.07 at room temperature, decreasing to 1.2 $\pm$ 0.1 at 700 K (Fig. 8). The present calculations for dK/dT and C_V were used in eqn. (9) to obtain the temperature dependence. The value at 298 K reported here differs considerably from that of WATANABE (1982) because he used lower values for α, K and C_V. Least squares analysis gives the fit

$$\gamma_{Th} = 0.924 + 94.73/T + 57319/T^2, \quad (10)$$

which is valid between the 350 to 660 K range of the thermal expansivity determination. Extrapolation at temperatures below to 200 K and above to 1000 are probably less accurate than the uncertainty of $\pm$10% for γ_{Th} at intermediate temperatures.

The initial pressure derivative $d\gamma_{Th}/dP|_o$ at 298 K is calculated to be -0.0020 ± 0.0005/kbar by using the thermodynamic identity

$$\left.\frac{\partial\alpha}{\partial P}\right|_{T=298K} = \frac{1}{K_T^2}\left.\frac{\partial K_T}{\partial T}\right|_{P=1atm} \quad (11)$$

Because these cross derivatives are not known at high temperature or pressure, the pressure dependence of γ_{Th} cannot be calculated except by assuming a linear dependence (*i.e.*, that $d\gamma_{Th}/dP$ is constant).

These above values derived from thermodynamic properties can be compared to the weighted sum of the microscopic properties

$$\gamma_{ave}(T,P) = \Sigma\sigma(\nu_i,T)\gamma_i(P)/\Sigma\sigma(\nu_i,T) \quad (12)$$

where the Einstein functions are

$$\sigma(\nu_i,T) = \left(\frac{h\nu_i}{kT}\right)^2 \frac{\exp\left(\frac{h\nu_i}{k_T}\right)}{\left[1-\exp\left(\frac{h\nu_i}{k_T}\right)\right]^2} \quad (13)$$

Table 5. Thermodynamic properties of stishovite at pressure

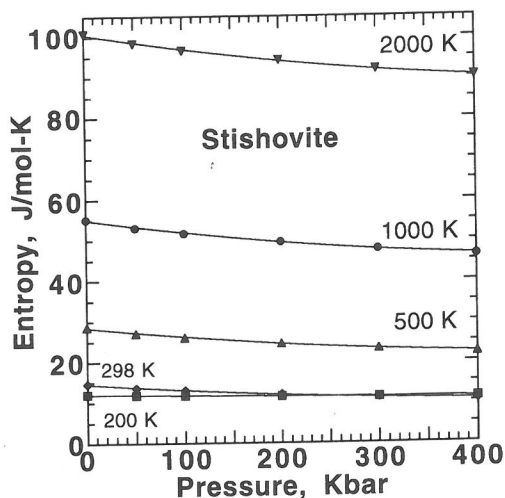| Temp. K	C_V Joule/mole-K	S_V Joule/mole-K
200	27.107-0.0198 P+1.69x10^{-5} P^2	11.98-0.0033 P+2.73x10^{-6} P^2
298	42.491-0.0196 P+1.46x10^{-5} P^2	14.51-0.0173 P+1.87x10^{-6} P^2
500	59.198-0.0125 P+7.27x10^{-6} P^2	28.37-0.0249 P+2.35x10^{-5} P^2
1000	70.250-0.00349 P	54.95-0.0338 P+3.09x10^{-5} P^2
2000	73.691-0.000971 P	100.54-0.0393 P+3.37x10^{-5} P^2

P is in kbar.

FIG. 10. Calculated entropy (S_V) as a function of pressure. Symbols are as in Fig. 9. At low temperature, S is essentially independent of pressure.

(e.g., KRISHNAN et al., 1979), k is Boltzman's constant and h is Planck's constant. The variation of γ_{ave} with temperature is not strong, such that above 700 K, γ_{ave} is roughly constant. Given this behavior and the need to estimate γ_i for the three inactive modes (Table 3), only the high temperature average of all optic modes of 1.15 ± 0.04 is reported here. Note that because E-type modes are doubly degenerate, these are counted twice in the average. Because estimates for mode gammas of the inactive modes are near the average values, the particular values chosen have a small effect on the computation. Averaging the slopes $d\gamma_i/dP$ gives $d\gamma_{ave}/dP = -0.0014$ with and estimated uncertainty of ± 0.0005. Because most of the vibrational modes depend linearly on pressure, and because the measured curvature is small, γ_{ave} will depend linearly on pressure, within the uncertainty stated above.

The calculated values of γ_{ave} and $d\gamma_{ave}/dP$ are equal to γ_{Th} at 700 K and to $d\gamma_{Th}/dP$ at 298 K, given the stated uncertainties. At 298 K, the average is much lower than γ_{Th}. The difference is due to the strong temperature dependence of γ_{Th} which stems from the strong temperature dependence of C_V. Because the microscopic average is essentially linear with pressure, assumption of constant $d\gamma_{Th}/dP$ is reasonable, which allows calculation of γ_{Th} at mantle conditions from eqn. (10) and the average value of the two derivatives $d\gamma/dP = -0.0017/kbar$.

CONCLUSIONS

Thermodynamic and elastic properties and their temperature and pressure derivatives were calcu-

lated for stishovite from measurements of vibrational spectra at pressure. A new method of obtaining the cross-derivative $dK/dT|_P$ was presented. In all cases, agreement with independently measured physical properties was excellent (i.e., equal within the stated uncertainties). The accuracy with which macroscopic properties can be determined from microscopic data suggests that the predicted 1 atm values for dK/dT, K'', dC_P/dP, dS/dP and $d\gamma_{Th}/dP$ are accurate and that formulations for all quantities presented here may be extrapolated to mantle conditions.

REFERENCES

ANDERSON O. L., CHOPELAS A. and BOEHLER R. (1990) Thermal expansivity versus pressure at constant temperature: a re-examination. Geophys. Res. Let. **17**, 685–688.

BASS J. D., LIEBERMANN R. C., WEIDNER D. J. and FINCH S. J. (1981) Elastic properties from acoustic and volume compression experiments. Phys. Earth and Planet. Int. **25**, 140–158.

BROUT R. (1959) Sum rule for lattice vibrations in ionic crystals. Phys. Rev. **113**, 43–44.

BURNS R. G. (1970) Mineralogical Applications of Crystal Field Theory. Cambridge University Press. Oxford, England.

BURNS R. G. (1985) Thermodynamic data from crystal field spectra. In Microscopic to Macroscopic: Atomic Environments to Mineral Thermodynamics. Rev. Mineral., Vol 14. (eds. S. W. KIEFFER and A. NAVROTSKY), p. 277–316. Mineralogical Society of America, Washington D.C.

BURNS R. G. and FYFE W. S. (1967) Crystal field theory and the geochemistry of transitions elements. In Researches in Geochemistry, Vol. 2. (ed. P. H. ABELSON) p. 259–285. J. Wiley and Son, New York.

CHANG Z. P. and BARSCH G. R. (1973) Pressure dependence of single-crystal elastic constants and anharmonic properties of spinel. J. Geophys. Res. **78**, 2418–2433.

CHAO E. C. T, FAHEY J. J., LITTLER J. and MILTON D. J. (1962) Stishovite, a very high pressure new mineral from Meteor Crater, Arizona. J. Geophys. Res. **67**, 419–421.

ENDO S., AKAI T., AKAHAMA Y., WAKATUSKI M., NAKAMURA T., TOMII Y., KOTO K. and ITO Y. (1986) High temperature x-ray study of single-crystal stishovite synthesized with Li_2WO_4 as flux. Phys. Chem. Miner. **13**, 146–151.

GILLET P., LE CLEAC'H A. and MADON M. (1990) High-temperature Raman spectroscopy of SiO_2 and GeO_2

polymorphs: anharmonicity and thermodynamic properties at high temperatures. *J. Geophys. Res.* **95**, 21635–21655.

HEMLEY R. J. (1987) Pressure dependence of Raman spectra of SiO₂ polymorphs: a-quartz, coesite, and stishovite. In *High Pressure Research in Mineral Physics* (ed. M. H. MANGHANI and Y. SYONO), p. 347–360. Terra Scientific Publishing Company, Tokyo.

HEMLEY R. J., MAO H. K. and CHAO E. C. T. (1986) Raman spectrum of natural and synthetic stishovite. *Phys. Chem. Miner.* **13**, 285–290.

HILL R. J, NEWTON M. D. and GIBBS G. V. (1983) A crystal chemical study of stishovite. *J. Solid State Chem.* **47**, 185–200.

HOFMEISTER A. M. (1991) Calculation of bulk moduli and their pressure derivatives from vibrational frequencies and mode Grüneisen parameters: solids with cubic symmetry or one-nearest-neighbor distance. *J. Geophys. Res.* **96**, 16181–16203.

HOFMEISTER A. M. (1995) Infrared microspectroscopy in the Earth Sciences. In *Practical Guide to Infrared Microspectroscopy* (ed. H. HUMICKI) p. 377–416. Marcel Dekker Inc., New York.

HOFMEISTER A. M. and CHOPELAS A. (1991) Thermodynamic properties of pyrope and grossular from vibrational spectroscopy. *Amer. Mineral.* **76**, 880–891.

HOFMEISTER A. M., XU J., MAO H. K., BELL P. M. and HOERING T. C. (1989) thermodynamics of fe-mg olivines at mantle pressures: Mid- and far-infrared spectroscopy at high pressure, *Amer. Mineral.* **14**, 281–306.

HOFMEISTER A. M., XU J. and AKIMOTO S. (1990a) Infrared spectroscopy of synthetic and natural stishovite. *Amer. Mineral.* **75**, 951–955.

HOFMEISTER A. M., HORIGAN J. and CAMPBELL J. A. (1990b) Infrared spectra of GeO₂ with the rutile structure and prediction of inactive modes for isostructural compounds. *Amer. Mineral.* **75**, 1238–1248.

HOLM J. L, KLEPPA O. J. and WESTRUM E. F. JR. (1967) Thermodynamics of polymorphic transformations in silica. Thermal properties from 5 to 1070 K and pressure-temperature stability fields for coesite and stishovite. *Geochim. Cosmochim. Acta* **31**, 2289–2307.

ISAAK D. G., ANDERSON O. L. and GOTO T. (1989) Measured elastic moduli of single-crystal MgO up to 1800 K. *Phys. Chem. Minerals* **16**, 704–713.

ITO H., KAWADA K. and AKIMOTO S. (1974a) Thermal expanstion of stishovite. *Phys. Earth and Planet. Int.* **8**, 277–281.

ITO H., KAWADA K. and AKIMOTO S. (1974b) *Erratum. Phys. Earth and Planet. Int.* **9**, 371.

JACKSON I. and NIESLER H. (1982) The elasticity of periclase to 3 GPa and some geophysical implications. In *High-Pressure Research: Applications in Geophysics* (ed. S. AKIMOTO and M. H. MANGHANI), p. 93–113. Academic Press, San Diego, CA.

KAHAN A., GOODRUM J. W., SINGH R. S. and MITRA S. S. (1971) Polarized reflectivity spectra of tetragonal GeO₂. *Jour. Appl. Phys.* **42**, 4444–4446.

KIEFFER S. W. (1979) Thermodynamics and lattice vibrations of minerals: 3. Lattice dynamics and an approximation for minerals with application to simple substances and framework silicates. *Rev. Geophys. Space Phys.* **17**, 20–34.

KIEFFER S. W. (1980) Thermodynamics and lattice vibrations of minerals: 4. Application to chain and sheet silicates and orthosilicates. *Rev. Geophys. Space Phys.* **18**, 862–886.

KINGMA K. J., COHEN R. E., HEMLEY R. J. and MAO H.-K. (1994) Novel signature of post-stishovite silica and implications for the Earth's mantle. *Nature* **374**, 243–245.

KRISHNAN R. S., SRINIVASAN R. and DEVANARAYANAN S. (1979) *Thermal Expansion of Crystals.* Permagon Press. Oxford, England.

MANGHNANI M. H. (1969) Elastic constants of single-crystal rutile under pressure to 7.5 kilobars. *J. Geophys. Res.* **74**, 4317–4328.

MAO H.-K., XU J. and BELL P. M. (1986) Calibration of the ruby pressure gauge to 800 kbar under quasi-hydrostatic conditions. *J. Geophys. Res.* **91**, 4673–4676.

NAGEL L. and O'KEEFFE M. (1971) Pressure and stress induced polymorphism of compounds with retile structure. *Mater. Res. Bull.* **6**, 1317–1320.

ROESSLER D. M. and ALBERS W. A. J. (1972) Infrared reflectance of single crystal tetragonal GeO2. *Jour. Phys. Chem. Solids* **33**, 293–296.

ROSS N. L., SHU J.-F., HAZEN R. M. and GASPARIK T. (1990) High-pressure crystal chemistry of stishovite. *Amer. Mineral.* **75**, 739–747.

SINCLAIR W. and RINGWOOD A. E. (1978) Single crystal analysis of the structure of stishovite. *Nature* **272**, 714–715.

STISHOV S. M. and POPOVA S. V. (1961) New dense polymorphic modification of silica. *Geokhimiya* **10**, 837–839.

SUMINO Y., NISHIZAWA O., GOTO T., OHNO I. and OZIMA M. (1977) Temperature variation of elastic constants of single-crystal forsterite between −190 and 400°C. *J. Phys. Earth* **25**, 377–392.

TRAYLOR J. G., SMITH H. G., NICKLOW R. M. and WILKINSON M. W. (1971) Lattice dynamics of rutile. *Phys. Rev. B* **10**, 3457–3472.

WATANABE H. (1982) Thermochemical properties of synthetic high-pressure compounds relevant to the Earth's mantle. In *High-Pressure Research: Applications in Geophysics* (ed. S. AKIMOTO and M. H. MANGHANI), p. 441–464. Academic Press, San Diego, CA.

WEIDNER D. J., BASS J. D., RINGWOOD A. E. and SINCLAIR W. (1982) The single-crystal elastic moduli of stishovite. *J. Geophys. Res.* **87**, 4740–4746.

WILLIAMS Q., HEMLEY R. J., KRUGER M. B. and JEANLOZ R. (1993) High-pressure infrared spectra of α-quartz, coesite, stishovite and silica glass. *J. Geophys. Res.* **98**, 22157–22170.

WOOTEN F. (1972) *Optical Properties of Solids.* Academic Press, Inc. San Diego.

YONEDA A. (1990) Pressure derivatives of elastic constants of single crystal MgO and MgAl₂O₄. *J. Phys. Earth* **38**, 19–55.